Inverse Scattering via Skin Effect

Yu Chen

Research Report YALEU/DCS/RR-1110
May 1996

YALE UNIVERSITY
DEPARTMENT OF COMPUTER SCIENCE

We present a stable method for the inverse scattering problem of the Helmholtz equation in two dimensions. The algorithm requires single-frequency scattering data, and is an iterative procedure which resembles the process of layer-stripping. The inversion method is based on the observation that the ill-posedness of the inverse scattering problem causes it to be almost linear in certain regimes. In these regimes, the algorithm solves the resulting quasi-linear equations to produce approximate solution to the inverse problem within a narrow circular layer surrounding the yet unrecovered part of the scatterer. This approximation is used to linearize the underlying narrow circular strip; in the process, the previously obtained solution is refined. The performance of the algorithm is demonstrated with several numerical examples for the special case of radially symmetric scatterers.

Inverse Scattering via Skin Effect

Yu Chen
Research Report YALEU/DCS/RR-1110
May 1996

The author was supported in part by the ONR under the grants ONR N00014-93-1-0114 and ONR N00014-94-1-0414.
Approved for public release: distribution is unlimited.
Keywords: *Inverse Scattering, Helmholtz Equation, Skin Effect, Layer-Stripping, Illuminated Areas, Recursive Linearization, Uncertainty Principle.*

1 Introduction

In [7], a stable method is presented that solves the inverse scattering problem for the Helmholtz equation in two dimensions. The algorithm is an iterative procedure, and requires multi-frequency scattering data. In this paper, we propose and test a single-frequency inversion method that solves the same inverse scattering problem.

There are two major difficulties in the solution of an inverse problem naturally formulated as a system of nonlinear equations: ill-posedness and local minima. They seem to act indissolubly together to make the investigation of the inverse problem even more difficult. Here is a typical situation where we are confronted with a dilemma. On one hand, the lower the frequency employed in the inversion, the fewer the local minima there are in the nonlinear system, but the more ill-posed the problem becomes. On the other hand, to reduce the ill-posedness and therefore to increase the resolution of the inversion, a relatively high frequency is desired; but the higher the frequency, the more numerous the local minima there are in the nonlinear system.

When high resolution is sought in a reconstruction, it can only be achieved with high-frequency. Therefore, the problem of local minima must be dealt with there. The fact that no optimization-based techniques have so far been made reliable shows that it is difficult to directly attack the problem. One of the well-known and systematic efforts made in solving the problem of local minima is the method of layer-stripping (see, for example, see [1], [2], [3]), in both the time and frequency domains. In this approach, the inverse, nonlinear problem is often reformulated as a nonlinear ordinary differential equation, usually of Riccati type in the frequency domain, for the scattering matrix in the context of inverse scattering (see [6]), or for the Dirichlet-to-Neumann mapping in the context of electrical impedance imaging (see [1], [3]). The measured data become the initial values of the ODE. The initial value problem is solved, which can be interpreted as layer-stripping the object being imaged, and the problem of local minima is simply eliminated. However, the propagation of the measured information into the object is unstable, for the initial value problem solved here is similar and connected to the Cauchy problem of the Laplace equation in the case of electrical impedance imaging, and of the Helmholtz equation in the case of inverse scattering, both being ill-posed.

The single-frequency inversion method to be presented in this paper, as well as the multi-frequency method of [7], is based on the observation that the ill-posedness of the inverse scattering problem causes it to be almost linear in certain regimes. In these regimes, the algorithm solves the resulting quasi-linear equations to produce approximate solution to the inverse problem within a narrow circular layer surrounding the yet unrecovered part of the scatterer. This approximation is used to linearize the underlying narrow circular strip; in the

process, the previously obtained solution is refined.

The underlying principle of physics used here is referred to as the skin effect. For elliptic partial differential equations in two (or higher) dimensions, a solution highly oscillating in a spatial direction decays or grows rapidly (usually exponentially) in directions perpendicular to it. This is the case for any oscillatory solution of the Laplace equation, or for an evanescent wave of the Helmholtz equation. Therefore, when the object is probed on its boundary with a wave highly oscillating across its circumference, only a thin layer of the object is penetrated, hence the term skin effect. Corresponding to this decaying incident field, the scattered field which we measure on the boundary contains information of the object in that thin layer. Such a measurement is entirely inadequate to determine the whole object—this obviously is a severely ill-posed problem. But the measurement may be used to approximately determine the object just in that thin layer. We can in fact do so since the problem of obtaining the thin layer from the measurement is essentially linear. That is how the recursive linearization process starts.

Less highly oscillatory incident waves are then irradiated onto the object. While the probing energy penetrates a thicker layer of the object, the relationship between the measurements and the parameters to be recovered in the deeper layer becomes more nonlinear. These nonlinear equations can be considered as perturbations to the already solved equations at the previous layers, and therefore can be continually and recursively linearized with the standard techniques of regular perturbations. Thus, the recursive linearization is a continuation method on a parameter of the the incident field (see (8) and the integer m there) which controls the depth of its penetration.

The inversion method is inherently multi-dimensional in the sense that in one-dimensional space the Cauchy problem for an elliptic equation is not ill-posed, that there is no decaying mode or skin effect there, and therefore that the method has no one-dimensional version. Also, had the problem not been ill-posed in two and higher dimensions, it might have been more difficult to design an algorithm to solve the inverse problem with numerous local minima.

The main purpose of this paper is to propose a single-frequency inversion method, and to demonstrate its preliminary numerical results. The plan of the paper is as follows: in Section 2, we reformulate the inverse scattering problem using the concept of illuminated areas; in Section 3, we describe the inversion method for the Helmholtz equation in two dimensions. In Section 4, we implement the method numerically for the special case of cylindrically symmetric scatterers, and present the numerical results. Finally, in Section 5, we conclude with brief remarks on the performance of the inversion algorithm and discuss its generalizations.

Remark 1.1 *Although our numerical experiments demonstrate convergence and*

stability of the inversion algorithm, its analysis is presently incomplete. Therefore, the results presented in this paper should be viewed as experimental.

2 Skin Effect and Illuminated Areas

In this section, we formulate the forward and inverse scattering problems for the Helmholtz equation

$$\Delta\phi(x) + k^2(1 + q(x))\phi(x) = 0 \tag{1}$$

in two dimensions, and describe the skin effect and related concepts.

2.1 The Scattering Problem

In (1), we assume that k is a positive number, and q is a smooth function with compact support $\Omega \subset \mathbb{R}^2$; we will be referring to the function q as the scatterer, or the forward model. We will be considering solutions of (1) of the form

$$\phi(x) = \phi_0(x) + \psi(x), \tag{2}$$

with ϕ_0 the incident, or the incoming, field satisfying in Ω the homogeneous Helmholtz equation

$$\Delta\phi_0(x) + k^2\phi_0(x) = 0, \tag{3}$$

and with ψ the scattered field subject to the outgoing (Sommerfeld) radiation condition

$$\lim_{r\to\infty} \sqrt{r}\left(\frac{\partial\psi}{\partial r} - ik\psi\right) = 0. \tag{4}$$

We will be referring to the determination of the scattered field from a given incoming field as a forward scattering problem. It is well-known (see, for example, [4]) that the forward scattering problem is well-posed.

It is also well-known that the scattering problem can be reformulated as the Lippmann-Schwinger equation for the scattered field ψ

$$\psi(x) = -k^2 \int_\Omega G_k(x,\xi)q(\xi)(\phi_0(\xi) + \psi(\xi))d\xi, \tag{5}$$

where G_k is the free-space Green's function for the Helmholtz equation. The inverse scattering problem is to determine the scatterer q inside the domain Ω from measurements of the scattered fields outside the scatterer. For definiteness, we assume that the measurements are taken on the boundary of Ω:

$$\{\ \psi(x)|_{x\in\partial\Omega}\ \}. \tag{6}$$

The inverse problem is nonlinear since both the scatterer and the scattered field is unknown inside Ω, and there is a product of them in the integral equation (5).

2.2 Skin Effect and Weak Scattering

For simplicity and without loss of generality, we assume that $\Omega \subset \mathbb{R}^2$ is a disk $D(\varpi)$ defined by the formula

$$D(\varpi) = \{ (x,y),\ \|(x,y)\| \leq \varpi \}, \tag{7}$$

for some $\varpi > 0$. As is well-known, inside $D(\varpi)$, the solutions of (3) are of the form

$$\phi_0^{(m)}(r,\theta) = J_m(kr) \cdot e^{im\theta}, \tag{8}$$

where m is integer, referred to as the propagation number hereafter; J_m is the Bessel function of order m, and $J_{-m} = (-1)^m J_m$. Furthermore, any incident field to $D(\varpi)$ is a linear combination of (8); therefore, we only need to consider (8) as the incident fields for the purpose of inverse scattering. For n greater than $k\varpi$, the Bessel function $J_n(kr)$ decays monotonically as the radius r decreases from ϖ to zero. In fact,

$$J_n(kr) \sim \frac{1}{\sqrt{2\pi n}} \left(\frac{e \cdot kr}{2n} \right)^n, \tag{9}$$

for kr substantially smaller than n. Therefore, for $|m|$ substantially greater than $k\varpi$, the incident field (8) decays rapidly in the neighborhood of $r = \varpi$. It can only penetrate the skin of the scatterer which interacts with the incident field, and produces a weak scattered field $\psi^{(m)}$. Thus, the Born approximation can be used to linearize the relationship between q and ψ. In other words, dropping the term containing the product of q and ψ in the Lippmann-Schwinger equation (5), to the second order of $\psi^{(m)}$, we have

$$\psi^{(m)}(x) = -k^2 \int_{D(\varpi)} G_k(x,\xi) q(\xi) \phi_0^{(m)}(\xi) d\xi, \tag{10}$$

for $|m|$ substantially greater than $k\varpi$. Note that the major contribution of the integral over $D(\varpi)$ comes from a thin layer of the disk near the boundary.

2.3 Illuminated Areas

As is shown in the preceding section, the incident field $\phi_0^{(m)}$ illuminates a thin layer of the scatterer for $|m|$ substantially greater than $k\varpi$. When $|m|$ decreases, the layer the incident field penetrates becomes thicker. In this section, we describe this process and introduce necessary notation.

As is well-known (see, for example, [5]), for an integer $n > 0$, $J_n(z)$ is an oscillatory function of z for $z > n$. It decays as z decreases in $[0,n]$, and it decays to zero at the rate z^n as z goes to zero. Therefore, given a small number $\epsilon > 0$, there exists $z_n > 0$ such that $|J_n(z)| \leq \epsilon$ for all $z \leq z_n$. Furthermore, z_n

is roughly of the order n, and decreases as n decreases. Therefore, in the disk $D(\varpi)$, the incident field

$$\phi_0^{(n)}(r,\theta) = J_n(kr) \cdot e^{in\theta} \tag{11}$$

illuminates an annular area

$$A_0(n,k) = \{\ (r,\theta) \mid r_n \leq r \leq \varpi\ \}, \tag{12}$$

where $k \cdot r_n = z_n$, and r_n decreases as n decreases. Figure 1 shows sixteen

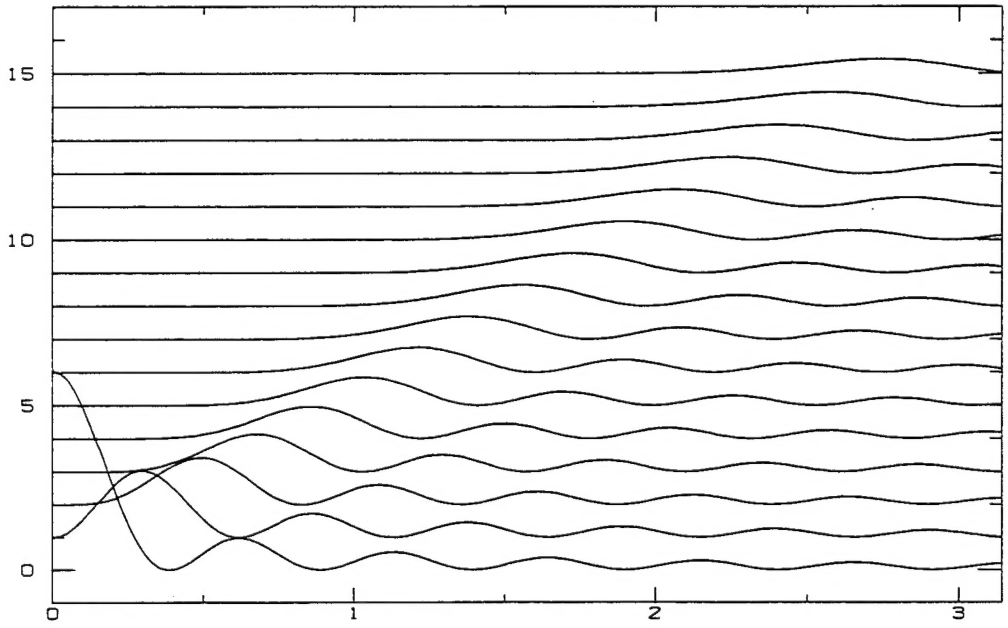

Figure 1: Absolute Values of the Incident Fields.

curves depicting $n + |\phi_0^{(n)}|$ for $n = 0, 1, \ldots, 15$, $k = 6.2$, as functions of the radius $r \in [0, \pi]$. For $n > 1$, the flat portion of each curve corresponds to the area that is near the center of the scatterer and is not illuminated by the incident field $\phi_0^{(n)}$. The area that is not illuminated by $\phi_0^{(1)}$ is essentially the center $r = 0$, whereas $\phi_0^{(0)}$ illuminates the entire scatterer.

Remark 2.1 *It is possible to rigorously define and calculate r_n, a process omitted here since it is tedious and its result is irrelevant to the subsequent discussions.*

Definition 2.2 *Let V be a domain in $\mathbb{R}^2$, and $g : V \mapsto \mathbb{C}$ a smooth function. For $\epsilon > 0$, we refer to*

$$\{\ (x,y),\ |g(x,y)| \geq \epsilon\ \} \subset V \tag{13}$$

as the ϵ-essential support of g. We will omit ϵ from the expression "ϵ-essential" if ϵ is a small number and its explicit reference there is superfluous.

It follows from Definition 2.2 that the area $A_0(n,k)$ illuminated by the incident field $\phi_0^{(m)}$ is the essential support of the incident field in $D(\varpi)$. We similarly define the illuminated area of the total field

$$\phi^{(m)} = \phi_0^{(m)} + \psi^{(m)} \tag{14}$$

as the essential support of the total field in $D(\varpi)$, and denote it by $\tilde{A}(m,k)$.

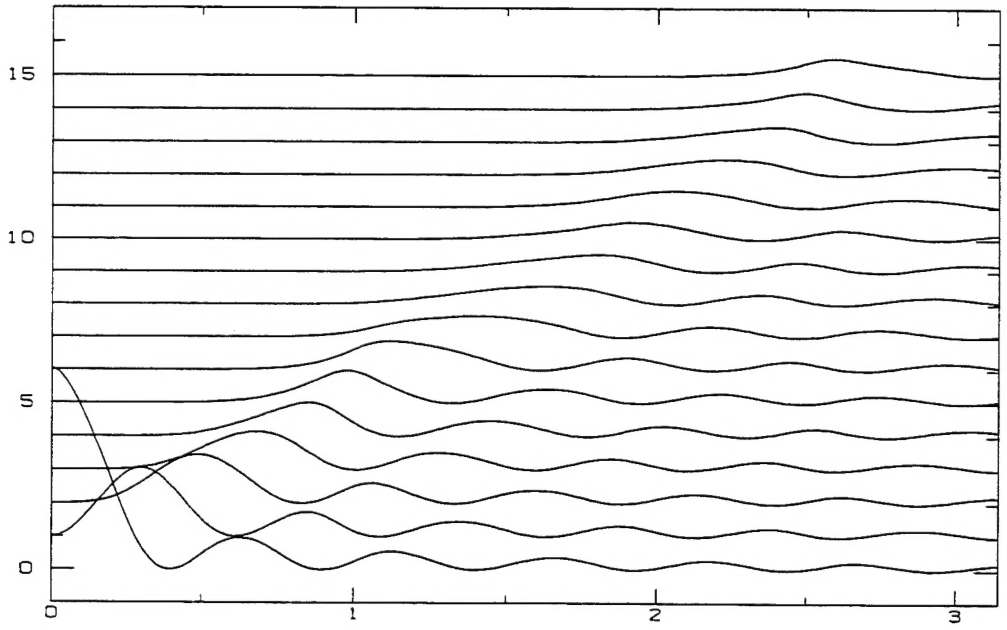

Figure 2: Absolute Values of the total Fields.

Therefore,

$$A(n,k) = \bigcup_{|m|\geq n} \tilde{A}(m,k) \tag{15}$$

is the illuminated area of the scatterer by the total fields

$$\{\ \phi^{(m)},\ |m| \geq n\ \}. \tag{16}$$

We also refer to $A(n,k)$ as the illuminated area by the scattering experiment with incident fields (16). Obviously, $D(\varpi) \supseteq A(0,k) \supseteq A(1,k) \supseteq A(2,k) \supseteq \ldots$.

Figure 2 shows sixteen curves depicting $n + |\phi^{(n)}|$ for $n = 0, 1, \ldots, 15$ as functions of the radius r, where $\phi^{(n)}$ is the total field corresponding to the forward

scattering problem with $\varpi = \pi$, $k = 6.2$ and a cylindrically symmetric scatterer q defined by the formula

$$q(r) = 0.26 \cdot [0.55\cos(4r) - 0.44\sin(8r) + 0.25\sin(12r) + 0.14\cos(16r)]. \quad (17)$$

For $n > 1$, the flat portion of each curve corresponds to the area that is near the center of the scatterer and is not illuminated by the total field $\phi^{(n)}$. The area that is not illuminated by $\phi^{(1)}$ is essentially the center $r = 0$, whereas $\phi^{(0)}$ illuminates the entire scatterer.

2.4 Reformulating the Inverse Scattering Problem

The essence of inversion is to determine a forward model $\check{q}$, which may not be the same as q, but which produces, exactly or approximately, the scattering measurement

$$\{ \psi^{(m)}(x)|_{x\in\partial D(k\varpi)} \} \quad (18)$$

in the scattering experiment with the incident field $\phi_0^{(m)}$ for all integer m. Moreover, for the sake of stability, we require that $\check{q}$ has small L^2 norm. In this section, we formalize these two requirements.

Definition 2.3 *Suppose that in a scattering experiment, the two forward models $q : \Omega \mapsto \mathbb{R}$ and $\check{q} : \Omega \mapsto \mathbb{R}$ produce respectively the two scattering measurements $\psi|_{\partial\Omega}$ and $\check{\psi}|_{\partial\Omega}$. For a given $\epsilon > 0$, the two scattering measurements are said to be ϵ-essentially the same if*

$$\|(\psi|_{\partial\Omega} - \check{\psi}|_{\partial\Omega})\|_2 \leq \epsilon. \quad (19)$$

We will omit ϵ from the expression "ϵ-essentially" if ϵ is meant to be a small number and its explicit reference there is superfluous.

Definition 2.4 *To a scattering experiment, the two forward models $\check{q}$ and $\check{q}$ are said to look (essentially) the same if they produce essentially the same scattering measurements in the experiment.*

Definition 2.5 *A forward model $\tilde{q}$ is said to be observable, or an observable part of the original scatterer q, to a scattering experiment at frequency k, if it looks the same as the original q, and its L^2 norm is the least among those that look the same as q.*

It follows from the Lippmann-Schwinger equation (5) and Definition 2.5 that an inversion using the incident fields

$$\{ \phi_0^{(m)},\ |m| \geq n \} \quad (20)$$

can only at best produce observable part of q in $A(n, k)$.

Definition 2.6 *Given an integer $n \geq 0$, we denote by $\check{E}(n)$ the scattering experiment with the incident fields (20), and by $\check{q}_n : A(n,k) \mapsto \mathbb{R}^1$ the observable part of q corresponding to the experiment $\check{E}(n)$ (here it is assumed that the observable forward model $\check{q}_n$ exists and is unique).*

With $\check{q}_n$ and $A(n,k)$, the scattering problem (5) can be modified as (see Remark 2.10)

$$\psi^{(m)}(x) = -k^2 \int_{A(n,k)} G_k(x,\xi)\cdot\check{q}_n(\xi)\cdot[\phi_0^{(m)}(\xi) + \psi^{(m)}(\xi)]d\xi, \tag{21}$$

for $|m| \geq n$. And therefore the inverse problem is to obtain $\check{q}_0$ which satisfies

$$\psi^{(m)}(x) = -k^2 \int_{A(0,k)} G_k(x,\xi)\cdot\check{q}_0(\xi)\cdot[\phi_0^{(m)}(\xi) + \psi^{(m)}(\xi)]d\xi, \tag{22}$$

with prescribed scattering data

$$\{\ \psi^{(m)}(x)|_{x\in\partial D(\varpi)},\ m \text{ integer }\}. \tag{23}$$

Remark 2.7 *More precisely, $\check{q}_0$ has the least L^2 norm among those forward models $\check{q}$ whose scattering data*

$$\{\ \check{\psi}^{(m)}(x)|_{x\in\partial D(\varpi)}\ \} \tag{24}$$

satisfy

$$\left(\sum_m \|(\psi^{(m)}|_{\partial D(\varpi)} - \check{\psi}^{(m)}|_{\partial D(\varpi)})\|_2^2\right)^{\frac{1}{2}} \leq \epsilon, \tag{25}$$

for a prescribed small number $\epsilon > 0$.

Remark 2.8 *Suppose that $\nu \neq 1$ is a positive number, and that the forward model $\tilde{q}$ is observable to the scattering experiment with the incoming fields*

$$\{\ \phi_{01},\ \phi_{02}\ \}, \tag{26}$$

whereas the forward model $\check{q}$ is observable to the scattering experiment with the incoming fields

$$\{\ \phi_{01},\ \nu\cdot\phi_{02}\ \}. \tag{27}$$

Then, the two forward models are not the same in general, because the cost functions (25) corresponding to the two sets of incident fields are different.

Remark 2.9 *In general, $\check{q}_n : A(n,k) \mapsto \mathbb{R}^1$ and $\check{q}_{n-1} : A(n-1,k) \mapsto \mathbb{R}^1$ are not identical in $A(n-1,k)$, but both look the same to the scattering experiment $\check{E}(n)$.*

Remark 2.10 *Corresponding to the incident field $\phi_0^{(m)}$, for $|m| \geq n$, the scattered field $\psi^{(m)}$ in (21) is actually dependent on n, and could have been denoted there by $\psi^{(m,n)}$. In other words, $\psi^{(m,n)}$ and $\psi^{(m,n-1)}$ are not the same in general, because they are the scattered fields corresponding to different forward models: $\check{q}_n$ and $\check{q}_{n-1}$. On the other hand, since both the forward models look the same as the original scatterer q, the two scattered fields $\psi^{(m,n)}$ and $\psi^{(m,n-1)}$ have the same value on the boundary of $D(k\varpi)$, which is the prescribed scattering data (18).*

2.5 A Continuous Version of the Propagation Number

The propagation number n of the total field

$$\phi^{(n)} = \phi_0^{(n)} + \psi^{(n)} \tag{28}$$

measures the depth of the illuminated area $A(n,k)$: the smaller it is, the deeper the total field penetrates the scatterer. Since $A(n,k)$ and $\check{q}_n$ depend on the discrete variable n, it is analytically improper to carry out perturbational analysis of $A(n,k)$ and $\check{q}_n$ on n. In this section, we generalize the propagation number n to a continuous variable η.

Given a real number $b > 0$ (the actual value of b is qualitatively unessential in the following discussion), consider a smooth function $\nu : \mathbb{R}^1 \mapsto \mathbb{R}^1$ defined by the formula

$$\nu(\eta) = \begin{cases} 0, & \eta \le -b, \\ 1, & \eta \ge 0, \\ \text{monotone}, & \eta \in [-b, 0]. \end{cases} \tag{29}$$

For $\eta \ge 0$, we denote by $\breve{E}(\eta)$ the scattering experiment with the weighted incident fields

$$u_0^{(m,\eta)} = \nu(|m| - \eta) \cdot \phi_0^{(m)} \tag{30}$$

for all integer m. We further denote by $\check{q}_\eta$ the observable part of q to the experiment $\breve{E}(\eta)$ (see Remark 2.8), and by $v^{(m,\eta)}$ the corresponding scattered field, so that

$$v^{(m,\eta)}(x) = -k^2 \int_{D(\varpi)} G_k(x,\xi) \cdot \check{q}_\eta(\xi) \cdot [u_0^{(m,\eta)}(\xi) + v^{(m,\eta)}(\xi)] d\xi. \tag{31}$$

It is easy to observe the following facts.

1. If $\eta > b$, the incident fields actually used in the experiment $\breve{E}(\eta)$ are not all but only those whose propagation numbers m are greater, in absolute value, than $\eta - b$.

2. If $\eta = \mathrm{N}$ is substantially greater than $k\varpi$, every incident field used in the experiment $\breve{E}(\eta)$ can only penetrate a thin layer of the scatterer. This means that for all $|m| > \mathrm{N} - b$ the Lippmann-Schwinger equation (31) can be replaced by the Born approximation (see Section 2.2)

$$v^{(m,\mathrm{N})}(x) = -k^2 \int_{D(\varpi)} G_k(x,\xi) \cdot \check{q}_\mathrm{N}(\xi) \cdot u_0^{(m,\mathrm{N})}(\xi) d\xi. \tag{32}$$

The observable forward model $\check{q}_\mathrm{N}$ can be obtained by solving these linear equations for given scattering data

$$\{\ v^{(m,\mathrm{N})}(x)|_{x \in \partial D(\varpi)},\ |m| > \mathrm{N} - b\ \}. \tag{33}$$

3. At $\eta = 0$, incident fields of all propagation numbers are used in the experiment, and they are equally weighted by the factor $\nu(|m|) = 1$. Therefore, the forward model $\check{q}_0$ is identical to $\check{q}_0$, both being the observable part of q corresponding to the same scattering experiment with all the incident fields

$$\{ \phi_0^{(m)}, \text{ for all integer } m \}. \tag{34}$$

Remark 2.11 *Clearly, for a small number δ, the scattering experiment $\check{E}(\eta - \delta)$ is a small perturbation to the experiment $\check{E}(\eta)$. More specifically, it follows from (30) that the incident field $u_0^{(m,\eta)}$ depends on η smoothly, and so do the scattered and total fields, due to the well-posedness of the forward scattering problem. In the reminder of the paper, we assume that $\check{q}_\eta$ also depends on η smoothly.*

3 Layer-stripping via Skin Effect

The aim of inverse scattering is to determine $\check{q}_n|_{n=0}$ (see Section 2.4, and Remark 2.7 therein), or equivalently, to determine $\check{q}_\eta|_{\eta=0}$ (see Section 2.5). The two forward models $\check{q}_\eta$ and $\check{q}_n$ depend on the two different parameters n and η, one being integer and therefore discrete, the other real number and therefore continuous. Accordingly, the iterative inversion method to be presented in this section has two versions: one determines $\check{q}_0$ via perturbational analysis on the continuous parameter η, the other determines $\check{q}_0$ on the discrete parameter n. Their descriptions are almost identical. Their numerical performances are similar. Both versions can be interpreted as layer-stripping the scatterer.

3.1 Recursive Linearization on η

The nonlinear inverse problem can be recursively linearized via a standard perturbational analysis, also known as the method of continuation, on η. It finds the forward model $\check{q}_\eta$ first for a large η where the nonlinear equations governing $\check{q}_\eta$ are essentially linear. The method then determines $\check{q}_{\eta-\delta}$ for a small number δ. The nonlinear equations governing $\check{q}_{\eta-\delta}$ can be linearized by those governing $\check{q}_\eta$. This process is repeated, and finally, $\check{q}_0$ is obtained. We describe the inversion method in the following four steps.

Step 1 (Initialization). Choose N sufficiently greater than $k\varpi$, and divide

Figure 3: Discretization of η.

the interval $[0, \mathrm{N}]$ into M sufficiently small chunks with the grid

$$\{ \eta_0, \eta_1, \cdots, \eta_{\mathrm{M}} \}, \tag{35}$$

where $\eta_0 = 0$, $\eta_{\mathrm{M}} = \mathrm{N}$, and $\eta_i < \eta_{i+1}$ for $0 \leq i < \mathrm{M}$. We intend to obtain $\breve{q}_\eta$ at $\eta = \eta_{\mathrm{M}}, \eta_{\mathrm{M}-1}, \cdots, \eta_0$.

Step 2 (Born Approximation). At $\eta = \eta_{\mathrm{M}} = \mathrm{N}$, obtain the observable forward model $\breve{q}_{\mathrm{N}}$ by solving the linear equations (32).

Remark 3.1 *The purpose of having a sufficiently large* N *is to attain the skin effect and therefore sufficiently weak scattering (see Section 2.2 for details) in order to make the Born approximation (32) more accurate. It turns out that the Born approximation needs not be very accurate in order to successfully implement Step 2. In numerical computation,* N *usually can be chosen only slightly greater than* $k\varpi$.

Remark 3.2 *In practice, the measurements of the scattered fields (33) on the boundary of* $D(\varpi)$ *are not available for* $|m| \gg k\varpi$, *for they correspond to evanescent waves; therefore, the linear equations (32) are solved for finite number of* m. *In numerical implementations, only two linear equations with* $m = \pm \mathrm{N}$ *are solved to produce an approximate forward model* $\breve{q}_{\mathrm{N}}$.

Step 3 (Linearization). Now, suppose that $\breve{q}_{\tilde{\eta}}$ has already been obtained where $\tilde{\eta} > 0$ is a point on the grid (35). We wish to determine $\breve{q}_\eta$ where η is the

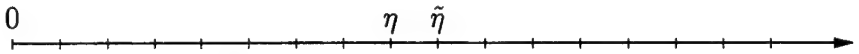

Figure 4: Update from $\tilde{\eta}$ to η.

grid-point immediately to the left of $\tilde{\eta}$. By definition, $\breve{q}_\eta$ is the forward model observable to the scattering experiment $\breve{E}(\eta)$ with the incident fields (30); therefore, the corresponding scattered field $v^{(m,\eta)}$ is connected to $\breve{q}_\eta$ by the Lippmann-Schwinger equation (see (31))

$$v^{(m,\eta)}(x) = -k^2 \int_{D(\varpi)} G_k(x,\xi) \cdot \breve{q}_\eta(\xi) \cdot [u_0^{(m,\eta)}(\xi) + v^{(m,\eta)}(\xi)] d\xi. \tag{36}$$

In (36), $\breve{q}_\eta$ and $v^{(m,\eta)}$ are unknown inside $D(\varpi)$, whereas $v^{(m,\eta)}(x)|_{x \in \partial D(\varpi)}$ is given as the scattering data.

3.1. On the other hand, in the same experiment $\breve{E}(\eta)$, the forward $\breve{q}_{\tilde{\eta}}$ produces a scattered field, denoted here by $\tilde{v}^{(m,\eta)}$ corresponding to the incident field $u_0^{(m,\eta)}$.

The scattered field satisfies the Lippmann-Schwinger equation

$$\tilde{v}^{(m,\eta)}(x) = -k^2 \int_{D(\varpi)} G_k(x,\xi)\cdot\breve{q}_{\tilde{\eta}}(\xi)\cdot[u_0^{(m,\eta)}(\xi) + \tilde{v}^{(m,\eta)}(\xi)]d\xi. \tag{37}$$

Since $\breve{q}_{\tilde{\eta}}$ is known, the forward problem (37) is solved for the scattered field; therefore, $\tilde{v}^{(m,\eta)}$ is known inside as well as on the boundary of $D(\varpi)$, for every m such that $|m| > \eta - b$.

3.2. By assumption, $\tilde{\eta} - \eta$ is small and $\breve{q}_\eta$ depends on η smoothly (see Remark 2.11); therefore the perturbations

$$\delta q = \breve{q}_{\tilde{\eta}} - \breve{q}_\eta, \tag{38}$$

$$\delta v^{(m)} = \tilde{v}^{(m,\eta)} - v^{(m,\eta)} \tag{39}$$

are also small. For every m such that $|m| > \eta - b$, subtracting (36) from (37), and omitting terms quadratic in δq and $\delta v^{(m)}$, we obtain an equation linking δq linearly to $\delta v^{(m)}$:

$$\delta v^{(m)}(x) = -k^2 \int_{D(\varpi)} G_k(x,\xi)\{\breve{q}_{\tilde{\eta}}\cdot\delta v^{(m)} + \delta q\cdot[u_0^{(m,\eta)} + \tilde{v}^{(m,\eta)}]\}(\xi)\cdot d\xi. \tag{40}$$

3.3. Denoting by K, $S_m : c(D(\varpi)) \mapsto c(D(\varpi))$ the two compact linear operators defined by the formulae

$$K(w)(x) = -k^2 \int_{D(\varpi)} G_k(x,\xi)\cdot\breve{q}_{\tilde{\eta}}(\xi)\cdot w(\xi)\cdot d\xi, \tag{41}$$

$$S_m(w)(x) = -k^2 \int_{D(\varpi)} G_k(x,\xi)\cdot[u_0^{(m,\eta)}(\xi) + \tilde{v}^{(m,\eta)}(\xi)]\cdot w(\xi)\cdot d\xi, \tag{42}$$

for arbitrary $w \in c(D(\varpi))$, we rewrite (40) as

$$\delta v^{(m)} = K(\delta v^{(m)}) + S_m(\delta q). \tag{43}$$

Since the forward scattering problem is well-posed, the operator $I - K$ is always invertible; thus

$$\delta v^{(m)} = (I - K)^{-1} \cdot S_m(\delta q). \tag{44}$$

3.4. Denote by $P : c(D(\varpi)) \mapsto c(\partial D(\varpi))$ the projection operator, and by $L_m : c(D(\varpi)) \mapsto c(\partial D(\varpi))$ the linear operator defined by the formula

$$L_m(w) = P \cdot (I - K)^{-1} \cdot S_m(w), \tag{45}$$

for arbitrary $w \in c(D(\varpi))$. Then the application of P on (44) yields

$$\delta v^{(m)}(x) = L_m(\delta q), \tag{46}$$

for all $x \in \partial D(\varpi)$, and all m such that $|m| > \eta - b$. Since the linear operator can be evaluated and therefore is known, and since $\delta v^{(m)}$ is known on the boundary $\partial D(\varpi)$ (see (36), (37), and (39)), the linear system (46) can be solved as a least-squares problem for δq. Finally, we obtain $\check{q}_\eta$ from $\check{q}_{\bar{\eta}}$ and δq via (38).

Remark 3.3 *In reality, $\delta v^{(m)}$ is not available for $|m| \gg k\varpi$ (see Remark 3.2); therefore, only a finite numbers of the linear equations (46) need to be solved. In numerical implementations, the linear equations with $\eta - b < |m| \leq \mathrm{N}$ are solved to produce an approximate forward model $\check{q}_\eta$.*

Step 4 (Recursion). The process of linearization described in Step 3 can obviously be iterated in two directions. First, the solution $\check{q}_\eta$ is accurate to the second order of δq; the approximation can be improved by replacing $\check{q}_{\bar{\eta}}$ with $\check{q}_\eta$ and repeating the computations in Step 3. Secondly, when a satisfactory solution $\check{q}_\eta$ is obtained at $\eta = \eta_i$, it is used in Step 3 to determine the next forward model $\check{q}_\eta$ at $\eta = \eta_{i-1}$ until $\check{q}_0$ is found.

Remark 3.4 *It turns out that only a low accuracy of the solution $\check{q}_\eta$ is required in numerical computation to maintain convergence of the recursion on η. In practice, the iteration discussed in Step 4 to improve $\check{q}_\eta$ is often unnecessary.*

3.2 Recursive Linearization on n

In this subsection, we describe another recursive process, almost identical to that presented in the preceding subsection, which successively determines the forward models

$$\check{q}_n, \quad n = \mathrm{N}, \mathrm{N}-1, \ldots, 1, 0. \tag{47}$$

This linearization process is accomplished on the discrete propagation number n. Its procedures are parallel to those of the preceding subsection. We briefly present them here for completeness and for the reason that the numerical results given in Section 4 are produced using this version of the linearization method.

Step 1 (Initialization). Choose N sufficiently greater than $k\varpi$, so that the skin effect is attained (in practice, N is usually chosen just slightly greater than $k\varpi$, see Remark 3.1).

Step 2 (Born Approximation). Obtain the observable forward model $\check{q}_{\mathrm{N}}$ by solving the linear equation (10) with $m = \pm\mathrm{N}$.

Step 3 (Linearization). Now, suppose that $\check{q}_{n+1}$ has already been obtained where $n < \mathrm{N}$ is a positive integer. We wish to determine $\check{q}_n$ which is the forward model observable to the scattering experiment $\check{E}(n)$, and which satisfies

the equations (see (21))

$$-k^2 \int_{A(n,k)} G_k(x,\xi)\cdot\check{q}_n(\xi)\cdot[\phi_0^{(m)}(\xi)+\psi^{(m)}(\xi)]d\xi = \psi^{(m)}(x), \tag{48}$$

for all m such that $|m| \geq n$. In (48), $\psi^{(m)}$ is unknown inside $D(\varpi)$, but is given on the boundary of $D(\varpi)$ as the scattering data (see (23)).

3.1. In the same scattering experiment $\check{E}(n)$, the forward model $\check{q}_{n+1}$, which is known, produces the scattered field, denoted here by $\tilde{\psi}^{(m)}$, corresponding to the incident field $\phi_0^{(m)}$. Therefore, $\tilde{\psi}^{(m)}$ satisfies the equation

$$-k^2 \int_{A(n+1,k)} G_k(x,\xi)\cdot\check{q}_{n+1}(\xi)\cdot[\phi_0^{(m)}(\xi)+\tilde{\psi}^{(m)}(\xi)]d\xi = \tilde{\psi}^{(m)}(x), \tag{49}$$

and is obtained by solving the forward problem (49).

3.2. Assuming that $\check{q}_{n+1}$ is close to $\check{q}_n$ (see Remark 3.6), we observe that the perturbations

$$\delta q = \check{q}_{n+1} - \check{q}_n, \tag{50}$$

$$\delta\psi^{(m)} = \tilde{\psi}^{(m)} - \psi^{(m)} \tag{51}$$

are small. For every $|m| \geq n$, subtracting (48) from (49), and omitting terms quadratic in δq and $\delta\psi^{(m)}$, we obtain an equation linking δq linearly to $\delta\psi^{(m)}$:

$$-k^2 \int_{A(n,k)} G_k(x,\xi)\{\check{q}_{n+1}\cdot\delta\psi^{(m)} + \delta q\cdot[\phi_0^{(m)}+\tilde{\psi}^{(m)}]\}(\xi)\cdot d\xi = \delta\psi^{(m)}(x). \tag{52}$$

3.3. Denoting by $K,\ S_m : c(A(n,k)) \mapsto c(A(n,k))$ the two compact linear operators defined by the formulae

$$K(w)(x) = -k^2 \int_{A(n,k)} G_k(x,\xi)\cdot\check{q}_{n+1}(\xi)\cdot w(\xi)\cdot d\xi, \tag{53}$$

$$S_m(w)(x) = -k^2 \int_{A(n,k)} G_k(x,\xi)\cdot[\phi_0^{(m)}(\xi)+\tilde{\psi}^{(m)}(\xi)]\cdot w(\xi)\cdot d\xi, \tag{54}$$

for arbitrary $w \in c(A(n,k))$, we rewrite (52) as

$$\delta\psi^{(m)} = K(\delta\psi^{(m)}) + S_m(\delta q). \tag{55}$$

Since the forward scattering problem is well-posed, the operator $I-K$ is always invertible; thus

$$\delta\psi^{(m)} = (I-K)^{-1}\cdot S_m(\delta q). \tag{56}$$

3.4. Denote by $P : c(A(n,k)) \mapsto c(\partial D(\varpi))$ the projection operator, and by $L_m : c(A(n,k)) \mapsto c(\partial D(\varpi))$ the linear operator defined by the formula

$$L_m(w)(x) = P\cdot(I-K)^{-1}\cdot S_m(w), \tag{57}$$

for arbitrary $w \in c(A(n,k))$. Then the application of P on (56) yields

$$\delta\psi^{(m)}(x) = L_m(\delta q), \tag{58}$$

for all $x \in \partial D(\varpi)$, and all m such that $|m| \geq n$. Since the linear operator can be evaluated and therefore is known, and since $\delta\psi^{(m)}$ is known on the boundary $\partial D(\varpi)$ (see (48), (49), and (12)), the linear system (58) can be solved as a least-squares problem for δq. Finally, we obtain $\check{q}_n$ from $\check{q}_{n+1}$ and δq via (51).

Step 4 (Recursion). Repeat the linearization procedures in Step 3 till $n = 0$ where $\check{q}_0$ is obtained.

Remark 3.5 *In reality, $\delta\psi^{(m)}$ is not available for $|m| \gg k\varpi$ (see Remark 3.2); therefore, only finite numbers of the linear equations (58) need to be solved. In numerical implementation, the equations with $n \leq |m| \leq \mathrm{N}$ are solved to produce an approximate forward model $\check{q}_n$.*

Remark 3.6 *The perturbation δq of (50), unlike that of (38), can not be made arbitrarily small, since n in (50) is discrete. In fact, our numerical experiment shows that δq may not be small at all. This, in principle, makes the perturbational analysis invalid and may lead to divergence of the recursive linearization. It turns out that δq is small in $A(n+1,k)$, the illuminated area by the experiment $\check{E}(n+1)$; therefore, the perturbational analysis can be carried out there to linearize the relationship between $\delta q|_{A(n+1,k)}$ and $\delta\psi^{(m)}$. However, δq usually is not small in*

$$T(n,k) = A(n,k) \setminus A(n+1,k), \tag{59}$$

which is the area illuminated by $\check{E}(n)$ but not by $\check{E}(n+1)$, and which we refer to as the transition zone. Fortunately, this layer is dimly illuminated by the experiment $\check{E}(n)$, and across it the skin effect occurs. Therefore, in the transition zone, the Born approximation is valid (see Section 2.2) and it linearizes the relationship between $\check{q}|_{T(n,k)}$ and the scattered fields of (48); consequently, the relationship between $\delta q|_{T(n,k)} = \check{q}|_{T(n,k)}$ and $\delta\psi^{(m)}$ is also essentially linear. In summary, in spite of the fact that δq may not be small in $A(n,k)$, it is essentially linearly connected to $\delta\psi^{(m)}$, as is formulated in (52) and finally in (58).

3.3 Recursive Linearization with an Initial Guess

Neither of the inversion procedures described in Sections 3.1 and 3.2 requires an initial guess of the scatterer to start. But an initial guess can be incorporated into the inversion procedures and proves beneficial to the reconstruction (see Example 3, Section 4) if it is not a bad approximation to the scatterer to be recovered. Usually, an initial guess is produced with a method of inversion at a relatively

low frequency k, where low-frequency components of the scatterer are recovered (see [7] for more details and numerical examples). The inversion method used to obtain an initial guess could be the one presented in [7] or described here in this paper.

The introduction of the initial guess to the two inversion procedures of Sections 3.1 and 3.2 is straightforward. We take the latter as an example to describe it. The only modification is made in Step 2 of Section 3.2 where $\check{q}_N$ is written as

$$\check{q}_N = \check{q}_{initial} + \delta q. \tag{60}$$

Consequently, δq can be obtained by solving the linear equation (10) with $m = \pm N$. With $\check{q}_N$ known, we proceed to Step 3 without any further alterations to the algorithm.

4 Numerical Experiments with Radially Symmetric Scatterers

Both versions of the recursive linearization method (see Sections 3.1 and 3.2) were implemented numerically. But since their performances are very similar, we only present numerical results of the second version based on the discrete propagation number n.

Although the inverse scattering problem and its linearization are described in this paper in terms of the Lippmann-Schwinger integral equations, models based on other equations exist, for example, the Riccati equations (see [6], [7]). Since an accurate and reliable code solving the integral equations is not presently available to the author, the actual equations employed are the Riccati equations whose Born approximation (required in Step 2 of Section 3.2) and perturbational analysis (all the procedures in Step 3 of Section 3.2) are discussed in great details and implemented numerically in [7].

For reconstruction of a general two-dimensional scatterer of $N \times N$ wavelengths, it turns out that the algorithm based on the integral equations requires $O(N^5)$ operations, whereas the algorithm based on the Riccati equations requires $O(N^6)$ operations, an approach too expensive to be used in solving a problem with $N = 10$. In this section, therefore, we only present numerical results of inversion of cylindrically symmetric scatterers, for which the algorithm requires $O(N^3)$ operations. The numerical experiments for general scatterers will be presented later when the code for the integral equations is acquired

4.1 The Forward Problem

As is mentioned in the beginning of Section 4, the Riccati equations, instead of the Lippmann-Schwinger equations, are used in the forward modeling. A FORTRAN

code was written to solve the forward problem required in Step 3.1 of Section 3.2; see [7] for details of the numerical treatment of the Riccati equations. For a prescribed scatterer q, the forward problem is also solved to produce the synthetic scattering data (see (23)). The numerical solutions in both cases are accurate at least to four digits. For a cylindrically symmetric scatterer, the forward solve requires $O(N^2)$ operations.

4.2 The Least-squares Problem

Since the ill-posedness of the original nonlinear inverse problem is inherited by the linearized problem (58), it must be solved as a least-squares problem. This is easy because it is a linear problem, for which the standard conjugate gradient method was used (see [7] for more details). As with solving other least-squares problems, the conjugate gradient iterations must be carefully measured and terminated for the stability of the solution. Here, the stop condition is on the magnitude of the residual: the iterative procedure is terminated and the solution is obtained when the L^2 norm of the residual is comparable to, or not less than, the precision in which the forward problem is solved or the scattering measurement is collected. This is the only place in the inversion method where "regularization of ill-posedness" is numerically imposed.

4.3 Numerical Results

Several technical details regarding the presentation of the numerical results require explanations.

1. The radius ϖ of the disk scatterer is chosen as $\varpi = \pi$ for convenience, so that the number of wavelengths across the diameter of the disk is the wave number k.

2. In plots showing the results of reconstructions, the prescribed scatterer functions are depicted in solid curves, whereas the numerically reconstructed scatterers are represented by dotted curves.

3. The L^2 error of a reconstruction is defined by the formula

$$e_2 = \left(\frac{1}{\pi}\int_0^\pi [q(r) - \check{q}_0]^2 \cdot r \cdot dr\right)^{\frac{1}{2}}, \tag{61}$$

where $\check{q}_0$ is the reconstructed scatterer obtained at the end of the recursive algorithm (see Section 3.2).

4. Scattering data of various accuracies are used in the inversion to examine the stability of the algorithm. Scattering data of low precision is obtained from data of high precision by truncation. We say that the data is accurate to D digits

if each number in the high precision data is truncated to D digits. For instance, truncating the number 0.12345 to three digits yields 0.123.

Example 1. Reconstruct a scatterer defined by the formula

$$q(r) = 0.1 \cdot [1 - \cos(14r)], \tag{62}$$

inside $D(\pi)$. Four inversions were made at $k = 8.6$ using scattering data accurate to $D = 1,\ 2,\ 3,\ 4$ digits; see Table 1 for the L^2 error of the reconstructions. Figure 5 shows the reconstructed scatterer against the exact, for $D = 1,\ 2,\ 3,\ 4$. With $D = 3$, the process of layer-stripping is evidently shown in Figures 6—8 where the reconstructions of $\check{q}_n$ of (47) are plotted.

D	1	2	3	4
e_2	0.7450E-1	0.1719E-1	0.648E-2	0.598E-2

Table 1: Errors of Reconstructions with $D = 1, 2, 3, 4$, Example 1.

Example 2. Reconstruct a scatterer defined by the formula

$$q(r) = 0.26 \cdot [0.55\cos(4r) - 0.44\sin(8r) + 0.25\sin(12r) + 0.14\cos(16r)], \tag{63}$$

inside $D(\pi)$. Four inversions were made at frequency $k = 9.3$ with data accurate to, respectively, $D = 1,\ 2,\ 3,\ 4$ digits; see Table 2 for the L^2 error of the reconstructions. Four more inversions were also made separately at frequencies

D	1	2	3	4
e_2	0.181	0.421E-1	0.309E-1	0.198E-1

Table 2: Errors of Reconstructions at $k = 9.3$, $D = 1, 2, 3, 4$, Example 2.

$k = 2.0,\ 4.1,\ 6.2,\ 9.3$ with scattering data accurate to four digits. Table 3 shows the L^2 error of the reconstructions; Figures 9 and 10 show plots of the reconstructions and the error distributions. According to Heisenberg's uncertainty

k	2.0	4.1	6.2	9.3
e_2	0.691	0.332	0.155	0.172E-1

Table 3: Errors of Reconstructions at Various Values of k, Example 2.

principle (see [7]), only those Fourier modes of the scatterer q whose frequencies

are lower than or about $2k$ can be recovered in a reconstruction at wave number k. Therefore, at $k = 2.0$, only the first term of (63) is recovered; at $k = 4.1$, roughly the first two terms of (63) are recovered; at $k = 6.2$, roughly the first three terms of (63) are recovered; and at $k = 9.3$, all four terms are essentially recovered. In fact, if we regard the first term alone, the first two terms alone, and the first three terms alone as approximations to the scatterer function (63), then they approximate (63) with L^2 errors 0.701, 0.339, and 0.170, which closely match the errors of inversions given in Table 3.

At $k = 4.1,\ 6.2$, the reconstructions of the intermediate forward models $\check{q}_n$ of (47) in the recursive linearization process are shown in Figures 11 and 12. The corresponding plots at $k = 2.0,\ 9.3$ are not shown here because they are similar to those shown in Figures 11 and 12.

Example 3. Reconstruct a scatterer defined by the formula

$$q(r) = 0.2 \cdot [\sin(4r) + c_1 \cdot \sin(8r) + c_2 \cdot \sin(14r)], \tag{64}$$

with $c_1 = -0.846153846$, $c_2 = 0.153846154$. The scatterer was reconstructed at $k = 9.7$. Figure 13 shows plots of the reconstruction and the error distribution. Four more inversions were made with four different initial guesses q_{init1}, q_{init2}, q_{init3}, and q_{init4} defined by the formulae

$$q_{init1}(r) = 0.2 \cdot [\sin(4r) - c_1 \cdot \sin(8r)], \tag{65}$$

$$q_{init2}(r) = 0.2 \cdot [\sin(4r) - c_1 \cdot \sin(8r) + c_2 \cdot \sin(14r) + 0.1 \cdot \sin(13r)], \tag{66}$$

$$q_{init3}(r) = 0.2 \cdot [\sin(4r) - c_1 \cdot \sin(8r) + c_2 \cdot \sin(14r) + 0.1 \cdot \sin(18r)]. \tag{67}$$

$$q_{init4}(r) = 0.2 \cdot [\sin(4r) - c_1 \cdot \sin(8r) + c_2 \cdot \sin(14r) + 0.1 \cdot \sin(22r)]. \tag{68}$$

Table 4 shows the L^2 errors of the initial guesses and of the final reconstructions. Again according to Heisenberg's uncertainty principle (see [7]), the highest frequency of the Fourier modes of the scatterer that can be recovered is about $2k = 2 \times 9.7 = 19.4$; therefore, the mode $\sin(13r)$ or $\sin(18r)$ in the initial guess is recognizable in the scattering experiment and can be eliminated from the initial guess in the reconstruction, whereas the mode $\sin(22r)$ in q_{init4} is not observable to the scattering experiment and can not be eliminated from the initial guess in the reconstruction; see Table 4.

Init. Guess	None	q_{init1}	q_{init2}	q_{init3}	q_{init4}
e_2 (Init.)	1.0	0.114	0.732E-1	0.736E-1	0.744E-1
e_2 (Final)	0.133E-1	0.529E-2	0.262E-2	0.138E-1	0.673E-1

Table 4: Errors of Reconstructions with Initial Guesses, Example 3.

Example 4. Reconstruct a scatterer defined by the formula

$$q(r) = \begin{cases} 0.2 \cdot [\sin(4r) + c_1 \cdot \sin(8r) + c_2 \cdot \sin(14r)], & r \leq 2.2707, \\ 0 & 2.2707 < r \leq \pi, \end{cases} \tag{69}$$

with $c_1 = -0.846153846$, $c_2 = 0.153846154$. The scatterer function is identical to that of Example 3 for $r \leq 2.2707$, and there is a discontinuity across the circle $r = 2.2707$. The inversion was made at $k = 9.7$. As is expected, the Gibbs' phenomenon appears in the reconstructed scatterer near the discontinuity; see Figure 14 for plots of the reconstruction and the error distribution. The recovery of the intermediate forward models $\tilde{q}_n$ of (47) are shown in Figures 15—17.

5 Discussions

We have presented a new inversion method and its preliminary numerical results in the special case of cylindrically symmetric scatterers. In this section, we make several technical remarks on the numerical experiments provided in Section 4.3, and discuss possible directions of future investigation of the method.

1. Numerical implementations for general scatterers in two dimensions will be presented on a later date when a code solving the two-dimensional Lippmann-Schwinger equation is available. The extension of the inversion method to the problem of electrical impedance imaging, though straightforward, constitutes a separate topic, and will be investigated and presented separately. In this case, a disk containing the inhomogeneity is probed with electrical potential of the form

$$\phi_0(r, \theta) = r^m \cdot e^{im\theta}, \quad m \geq 0. \tag{70}$$

Therefore, every probing field with $m > 0$ is a decaying mode in any interval $[0, A]$. This means that the number of parameters which can be recovered, independent of the size of the scatterer, is limited. In many applications, even such a limited resolution is difficult to acquire, and, if attainable, would be useful.

2. The skin effect and the illuminated areas of various depth can be achieved in three dimensions and in geometries other than that of the disk used here in this paper. For example, in underwater environment where the transducers are restricted on the surface of water, we may use the incident waves of the form

$$\phi_0(x, y, z) = e^{imx+iny} \cdot e^{-pz}, \tag{71}$$

to attain the skin effect, where z is the depth of the ocean, m, n are real numbers such that $m^2 + n^2 > k^2$ so that $p = \sqrt{m^2 + n^2 - k^2}$ is a positive number. Therefore, $p > 0$ is a parameter which controls the depth of penetration of the incident

field. Recursive linearization can be carried out on the continuous parameter p for decreasing p till $p = 0$. Then the recursion may be on the real parameter l of the incident field

$$\phi_0(x, y, z) = e^{imx+iny} \cdot e^{ilz}, \tag{72}$$

for increasing l in the interval $[0, k]$.

3. The stability of the method is demonstrated by reconstructions with noise-corrupted scattering data in Examples 1 and 2. More stability tests were made, the results being similar to those presented here. The inversion method does not require the solution of unstable initial value problems which the standard layer-stripping algorithm must solve in order to recover the scatterer layer by layer. When the ill-posed and nonlinear inverse problem is recursively linearized, the ill-posedness is passed to each linear problem which we know very well how to solve to maintain stability. Thus, the issue of stability is trivial here so far as we do not insist on recovering modes of the scatterer that are not observable to our scattering experiment. Conversely, if somehow during the recursive precess the intermediate result is polluted with such unobservable modes, usually high-frequency modes, there is no mechanism of the algorithm that can remove them, as is shown in Example 3.

4. The algorithm starts by illuminating the scatterer with an incident wave of high propagation number that penetrates only a thin layer of the scatterer. There, the measurement of the scattered field is weak, and therefore is prone to contaminations of noise. In principle, the propagation number m is required to be considerably greater than $k\varpi$ (see Section 2.2) in order to make the relationship between the measurement and the scatterer essentially linear. In practice, fortunately, only a roughly linear relationship is needed to produce an approximate observable forward model in the first layer. More precisely, the highest propagation number m can be chosen only slightly greater than $k\varpi$ such that the measurement of the far-field can be 10%—30% as strong as the strongest measurement of all propagation numbers. Thus, the so-called weak scattering required theoretically to attain ideal linearization does not practically cause problem to the noise-to-signal ratio: if the strongest scattering can be measured accurately, so can the weakest.

References

[1] J. Somersalo, M. Cheney, D. Isaacson and E. L. Isaacson (1991), *Layer stripping: A Direct numerical method for impedance imaging,* Inverse Problems 7 899–926.

[2] J. P. Corones *et. al.* (1992), *Invariant Embedding and Inverse Problems,* SIAM, Philadelphia.

[3] J. Sylvester (1992), *A Convergent Layer Stripping Algorithm for the Radially Symmetric Impedance Tomography Problem, Communications in PDE***17**,No.12, pp.1955–1994.

[4] D. Colton and R. Kress (1983), *Inverse Acoustic and Electromagnetic Scattering Theory,* Wiley-Interscience Publication, New York.

[5] G. Matviyenko (1992), *On the Evaluation of Bessel Functions,* Research Report 903, Department of Computer Science, Yale University.

[6] Y. Chen and V. Rokhlin (1995), *On the Riccati Equations for the Scattering Matrices in two dimensions,* Technical Report 1081, Department of Computer Science, Yale University.

[7] Y. Chen (1996), *Inverse Scattering via Heisenberg's Uncertainty Principle,* Technical Report 1091, Department of Computer Science, Yale University.

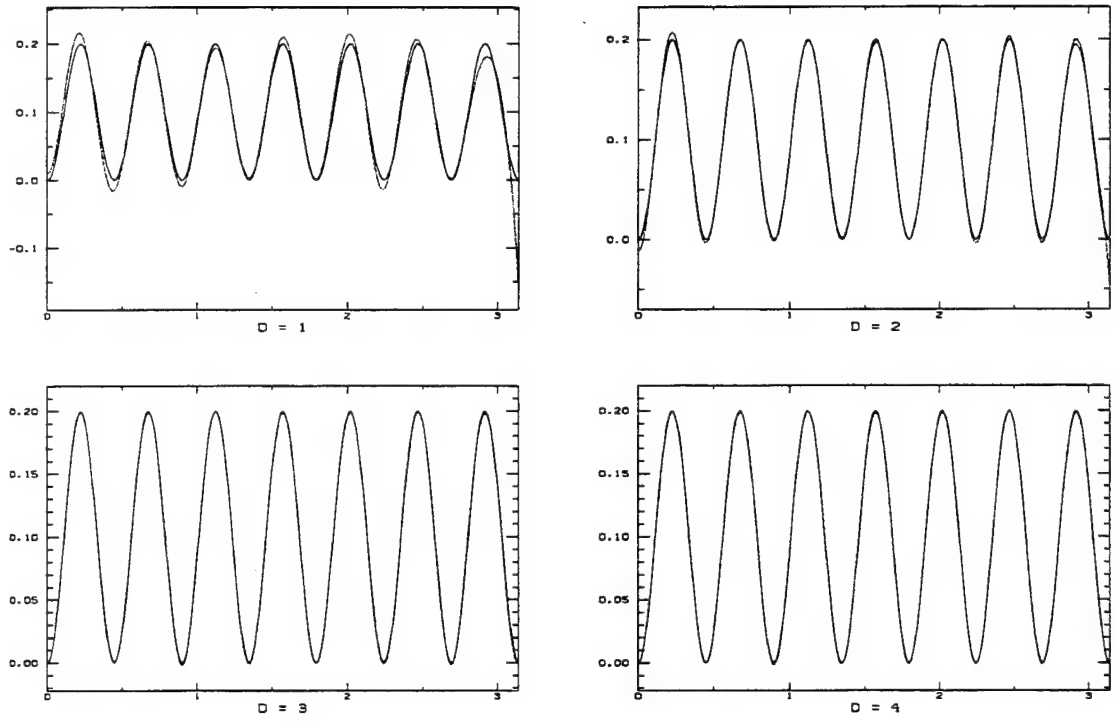

Figure 5: Reconstructions at $k = 8.6$, $D = 1, 2, 3, 4$, Example 1.

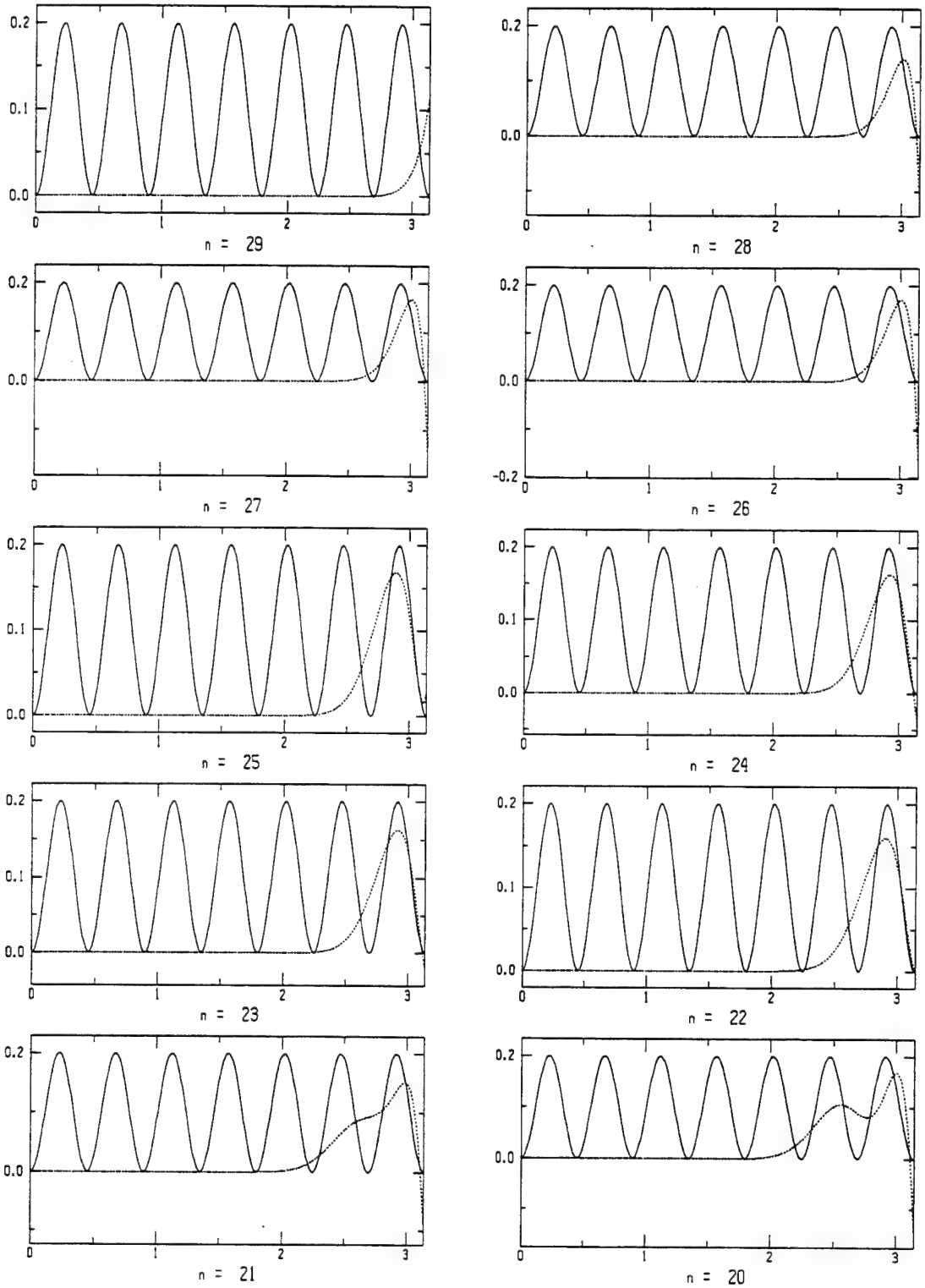

Figure 6: Reconstructions of q_n at $k = 8.6$, $n = 29, 28, \ldots, 20$, Example 1.

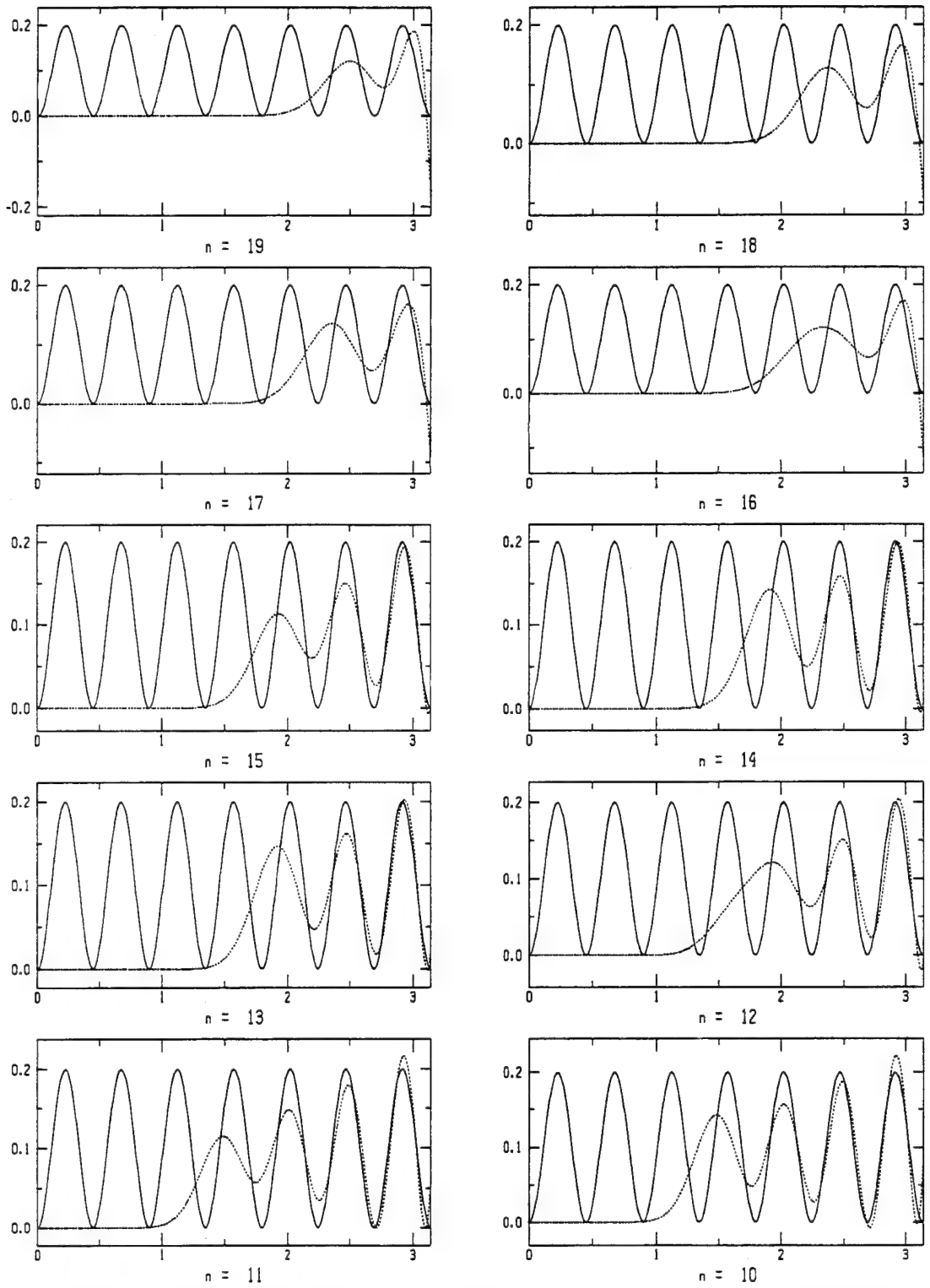

Figure 7: Reconstructions of q_n at $k = 8.6$, $n = 19, 18, \ldots, 10$, Example 1.

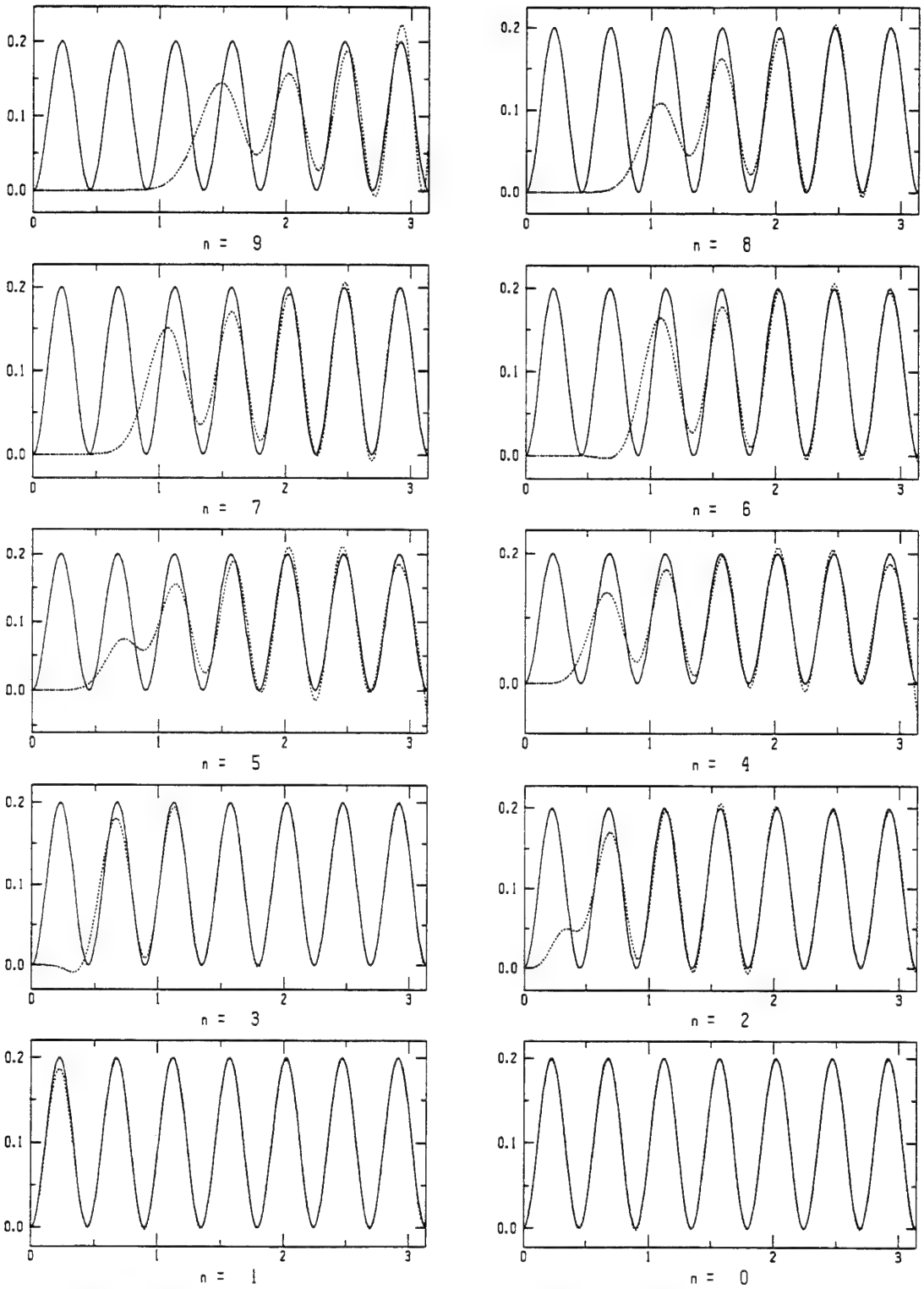

Figure 8: Reconstructions of q_n at $k = 8.6$, $n = 9, 8, \ldots, 0$, Example 1.

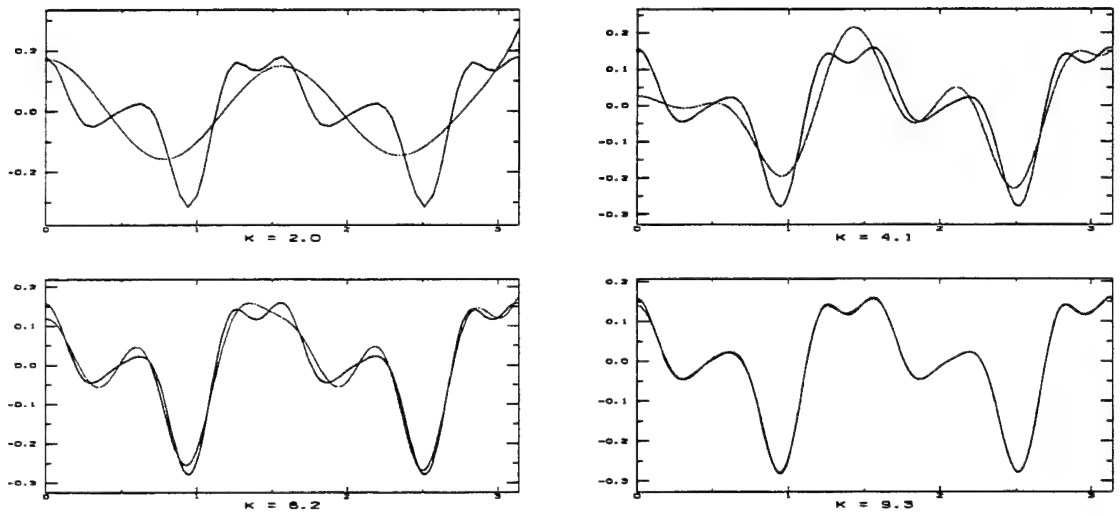

Figure 9: Reconstructions at $k = 2.0,\ 4.1,\ 6.2,\ 9.3,$ Example 2.

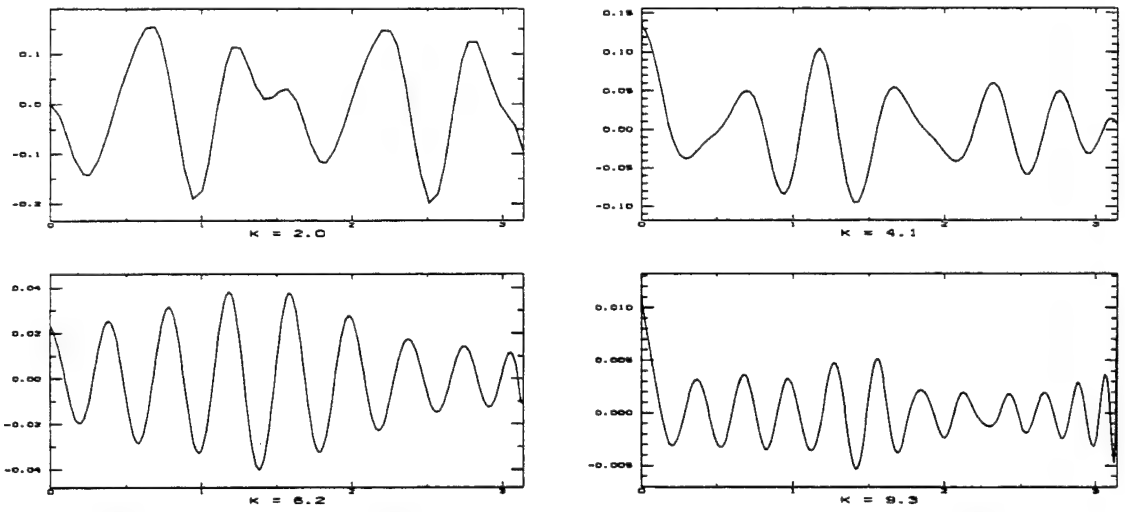

Figure 10: Errors of Reconstructions at $k = 2.0,\ 4.1,\ 6.2,\ 9.3,$ Example 2.

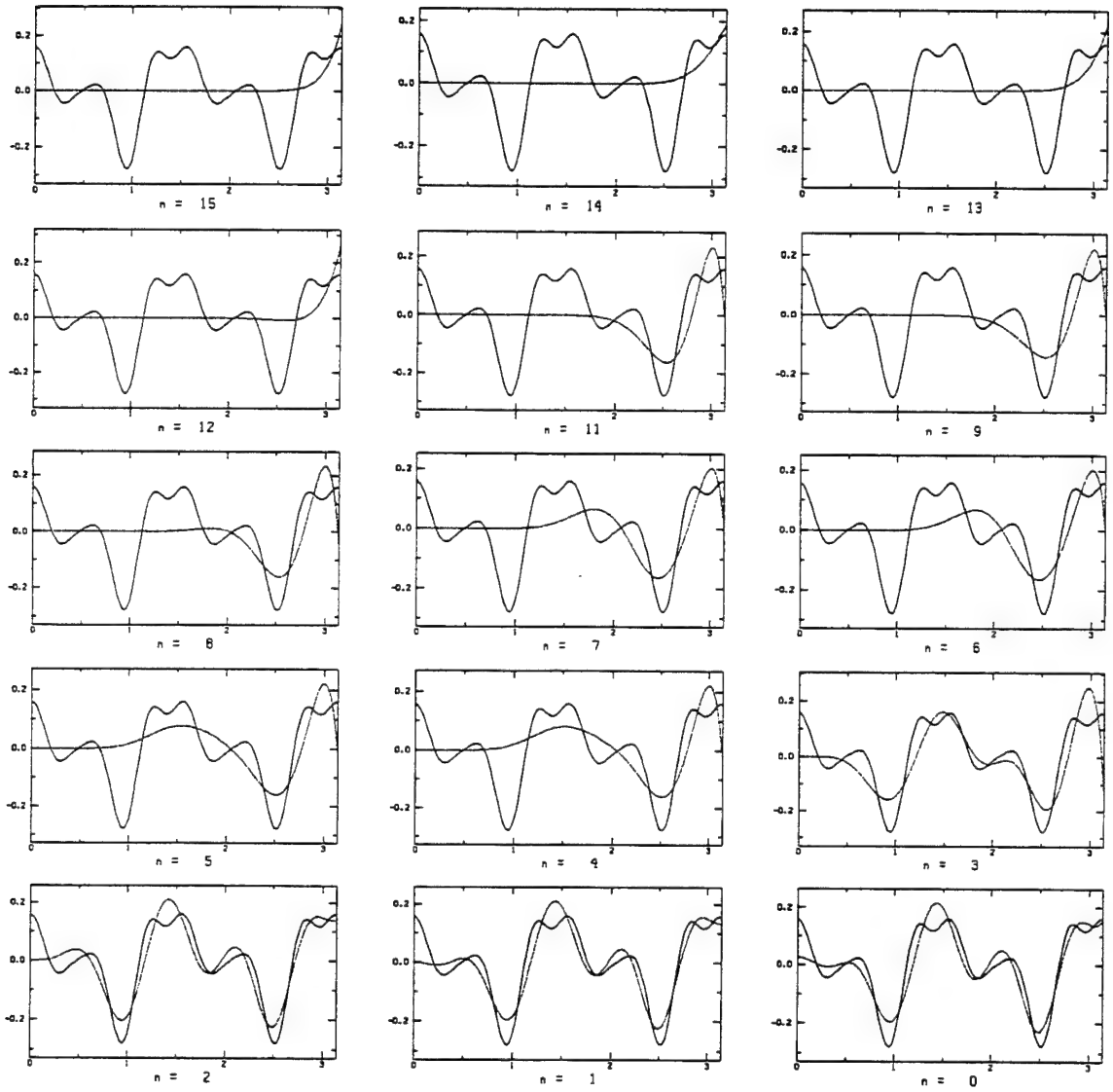

Figure 11: Reconstructions of q_n at $k = 4.1$, $n = 15, 14, \ldots, 0$, Example 2.

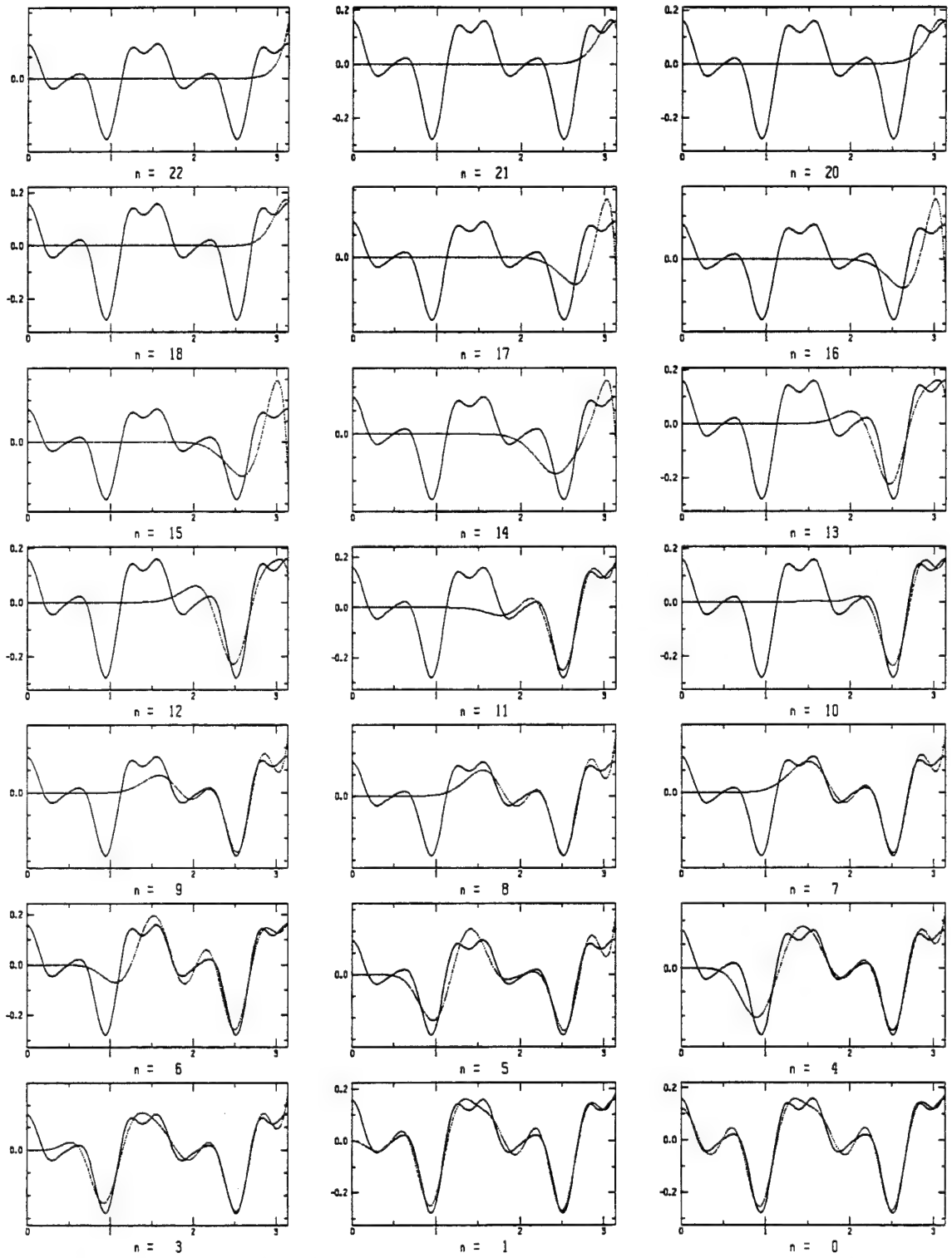

Figure 12: Reconstructions of q_n at $k = 6.2$, $n = 22, 21, \ldots, 0$, Example 2.

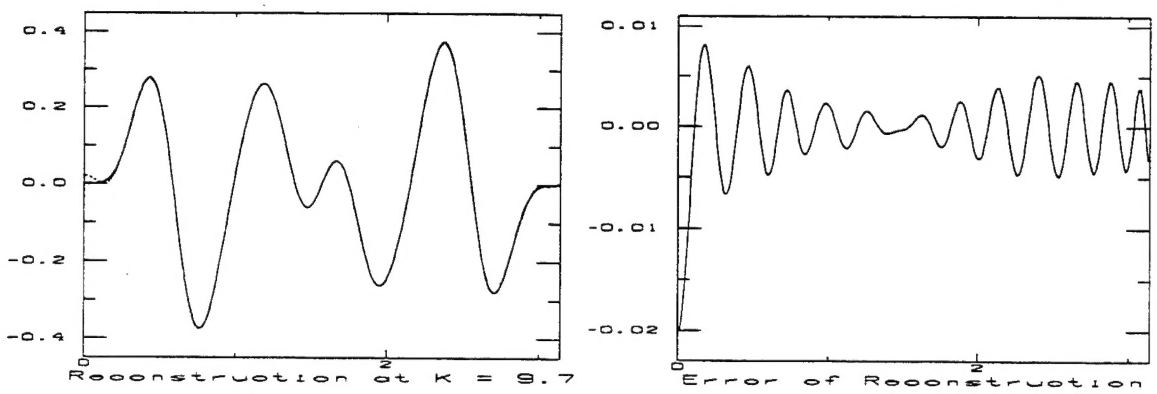

Figure 13: Reconstruction and Error Function, Example 3.

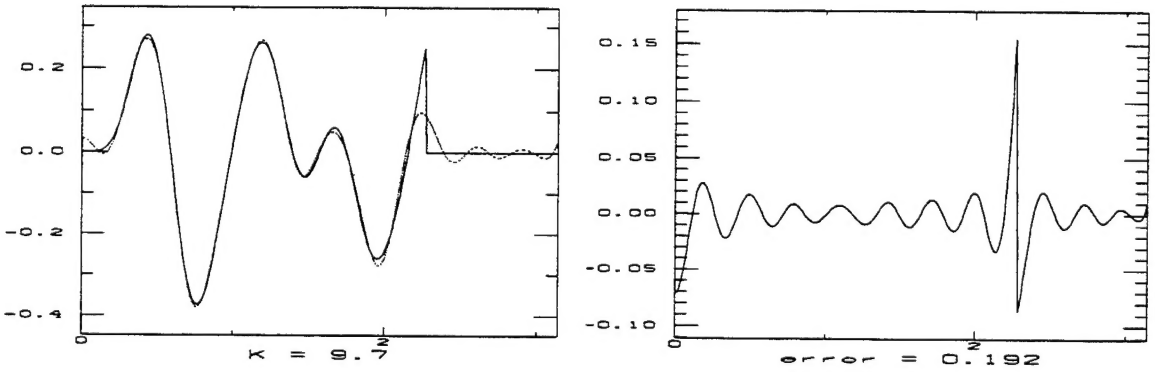

Figure 14: Reconstruction and Error Function, Example 4.

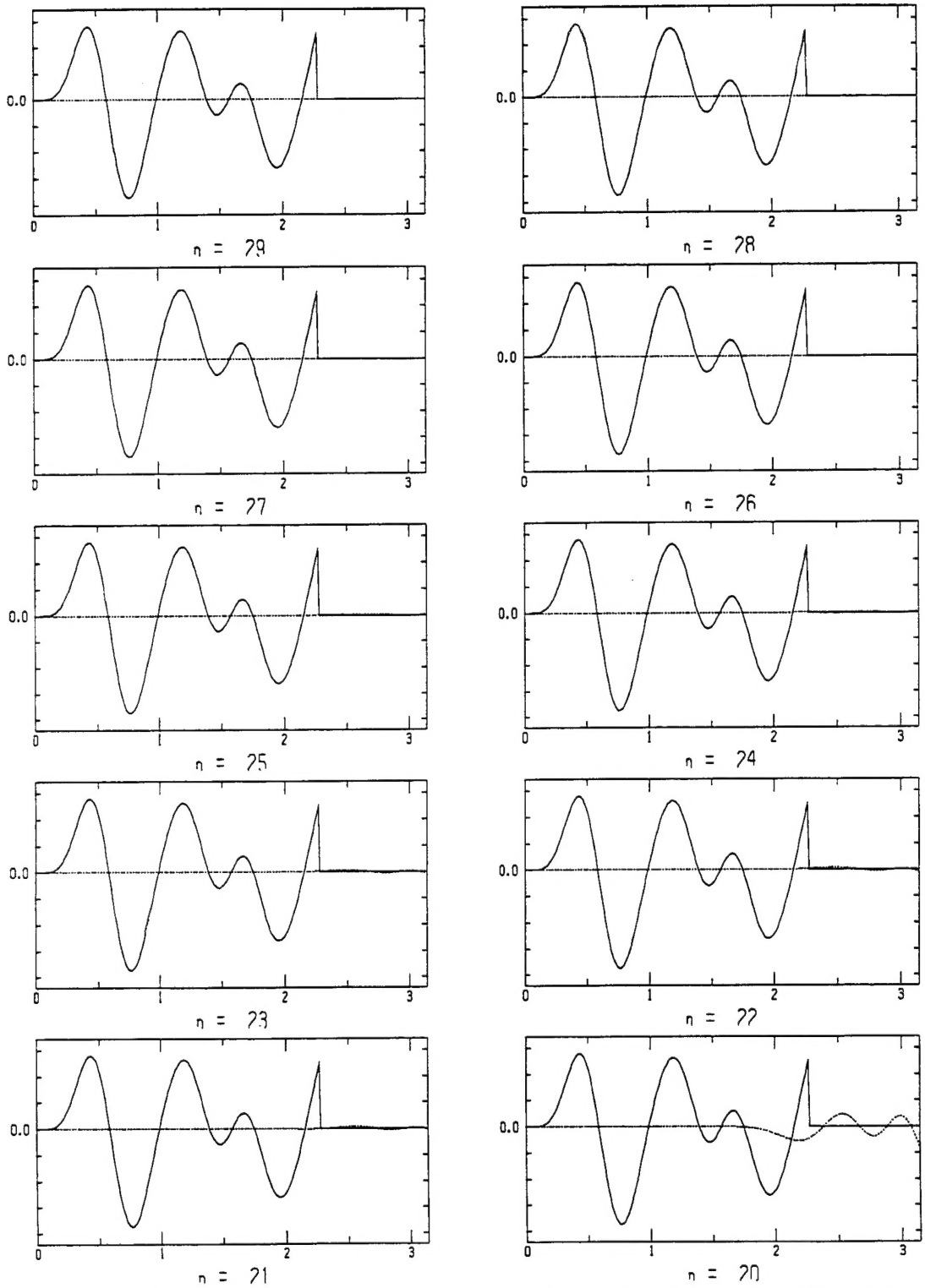

Figure 15: Reconstructions of q_n at $k = 9.7$, $n = 29, 28, \ldots, 20$, Example 4.

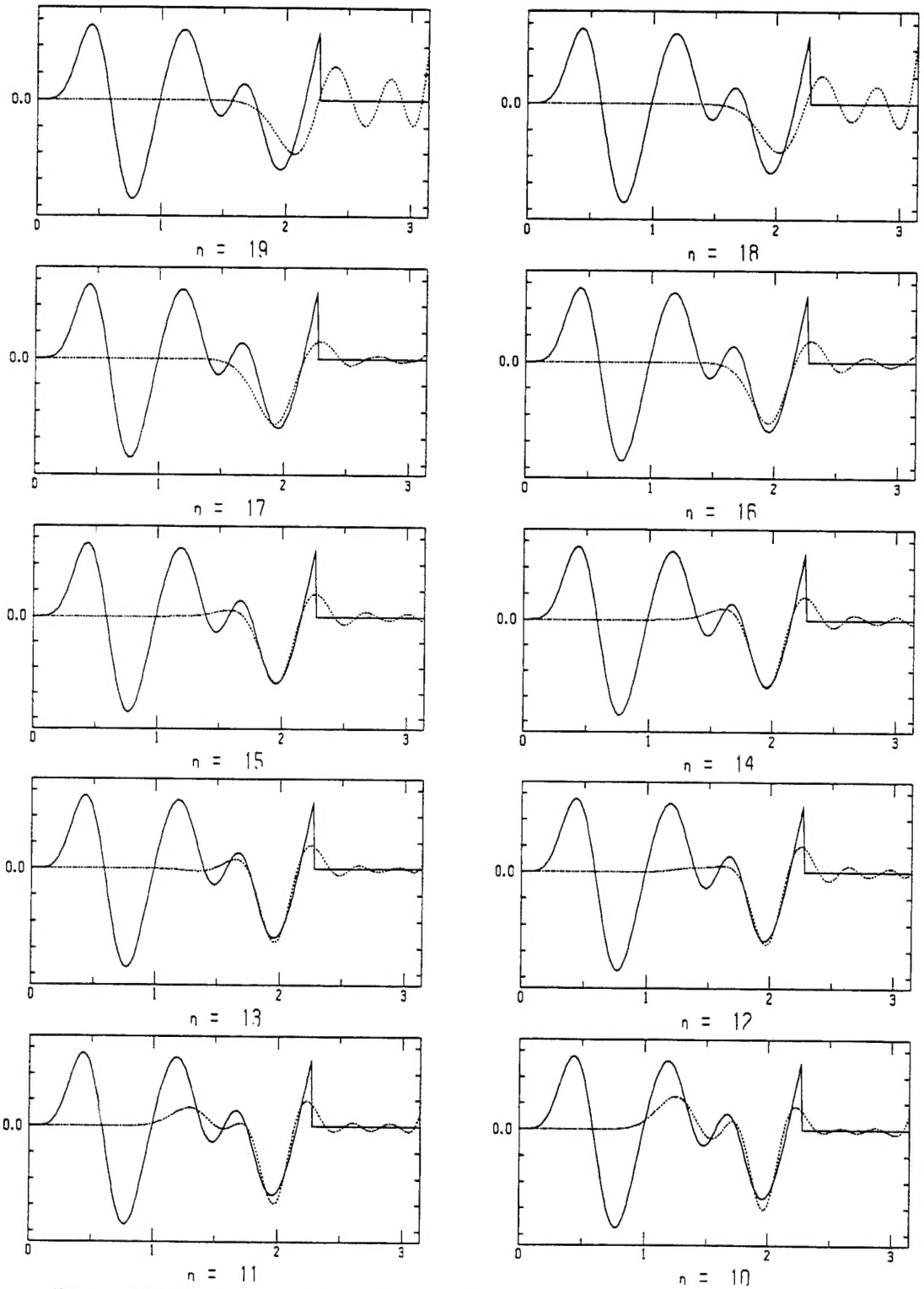

Figure 16: Reconstructions of q_n at $k = 9.7$, $n = 19, 18, \ldots, 10$, Example 4.

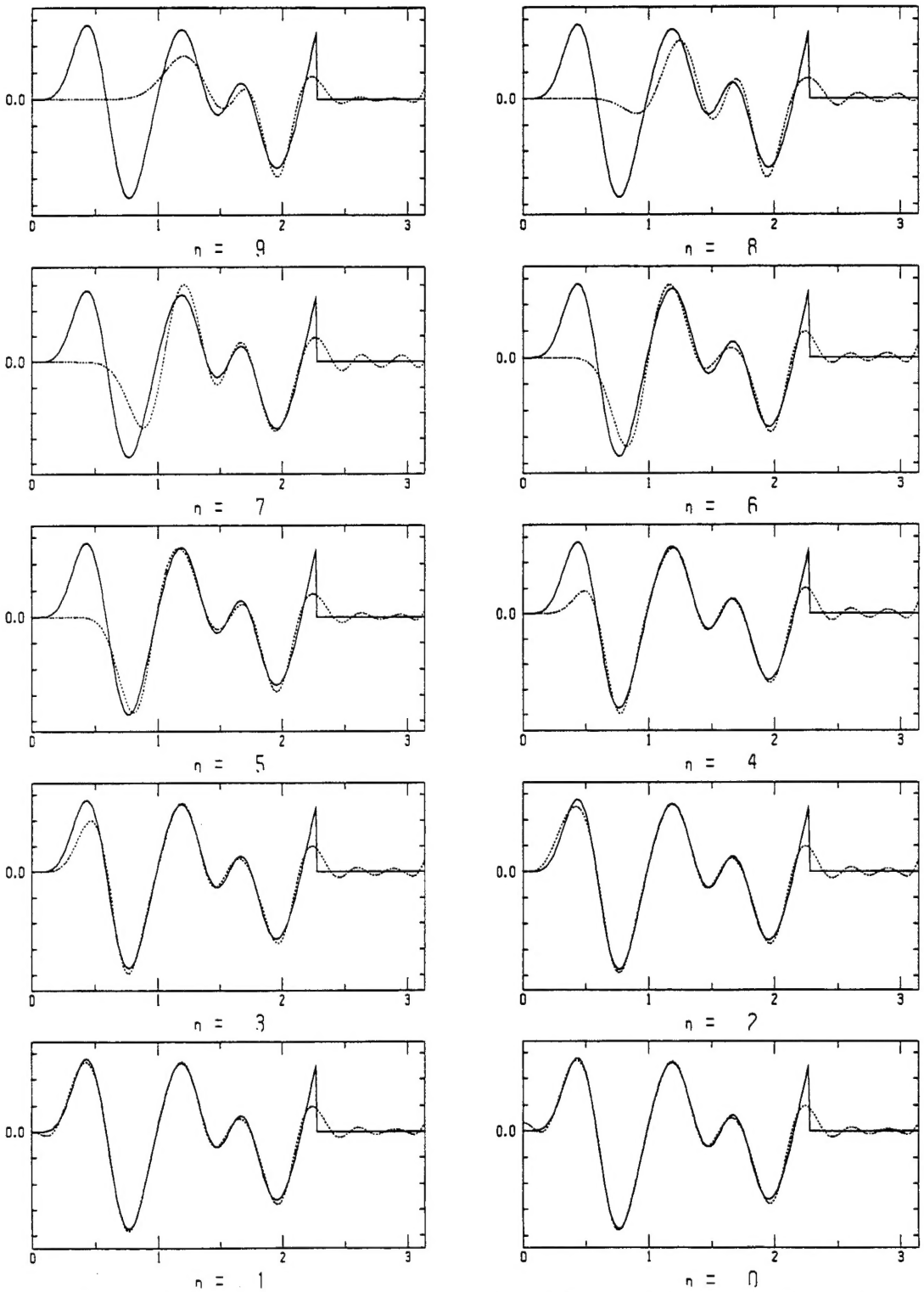

Figure 17: Reconstructions of q_n at $k = 9.7$, $n = 9, 8, \ldots, 0$, Example 4.